ICANS-VI

INTERNATIONAL COLLABORATION ON ADVANCED NEUTRON SOURCES

June 27 - July 2, 1982

THERMOFLUID DYNAMICS OF THE LIQUID LEAD-BISMUTH TARGET FOR THE SPALLATION NEUTRON SOURCE AT SIN

Y. Takeda
Schweizerisches Institut für Nuklearforschung
CH-5234 Villigen, Switzerland

ABSTRACT

Natural convection of liquid Lead-Bismuth Eutectics (LBE) has been numerically simulated and thermal-fluid behaviours of a target were studied. The calculation was based on the Boussinesq approximation and made for a simple geometry of a vertical cylindrical container with a distributed internal heat generation. Studies have been made of the effects of the target height, beam power and adiabatic side wall. They showed that the natural convection is effective for transporting heat and the vertical cylindrical target is practicable.

THERMOFLUID DYNAMICS OF THE LIQUID LEAD-BISMUTH TARGET FOR THE SPALLATION NEUTRON SOURCE AT SIN

Y. Takeda
Schweizerisches Institut für Nuklearforschung
CH-5234 Villigen, Switzerland

1. INTRODUCTION

The spallation neutron source at SIN is planning to use Lead-Bismuth Eutectics (LBE) in a liquid state as a target material [1]. Since the proton beam power is quite high (MW level), the choice of a liquid target seems attractive from the standpoint of heat removal. Furthermore it is planned to have a vertical target with beam entry from the bottom. The principle of this idea is to utilize the natural convection of LBE to transport the heat deposited by the beam in the lower part of the target, to a heat exchanger at the top. In spite of the attractions of a liquid target for high current beams from accelerators, hydrodynamic investigations are not plentiful. In the German project [2], pumped liquid metal was an alternative candidate for the target, and experimental and theoretical investigations were carried out. At TRIUMF, the lead target is in a partially molten state during operation. Calculations including natural convection were done [3] for this horizontal cylindrical target, and this seems to be the only thermofluid dynamical analysis of natural convection in a liquid target.

The principal difficulties of the problem are as follows:

(i) natural convection is in a completely confined space which allows no use of boundary layer theory,
(ii) the very low Prandtl number of liquid metal,
(iii) a difficulty in defining the Grashof number because of the distributed internal heat generation,
(iv) a fairly large aspect ratio (height/radius) which may lead to hydrodynamic instability,
(v) high power deposition.

A further result of the difficulties is that they can lead the flow regime into the turbulent region. For turbulent flow, it is very difficult to obtain an analytical prediction for an optimal design of the target. There exist a very limited number of reports of experimental work for turbulent natural convection of liquid metal.

In the present work, the numerical simulation was performed for natural convection of LBE in a vertical cylindrical container of finite length, in order to examine the general thermofluid behaviours.

2. CALCULATIONAL METHOD

2.1 Assumptions

In formulating the problem, the following assumptions were adopted:

(i) All the physical phenomena are axis-symmetric, and the beam profile does not change during irradiation, so that the problem is treated in a two-dimensional system.
(ii) The flow is laminar.
(iii) The Boussinesq approximation is valid, that is, all the physical properties are constant except for those affecting the buoyancy force.
(iv) The LBE is always molten so as to avoid the moving boundary problem.

The coordinate system used is shown in Fig. 1. Only the half plane of the vertical cross section is shown.

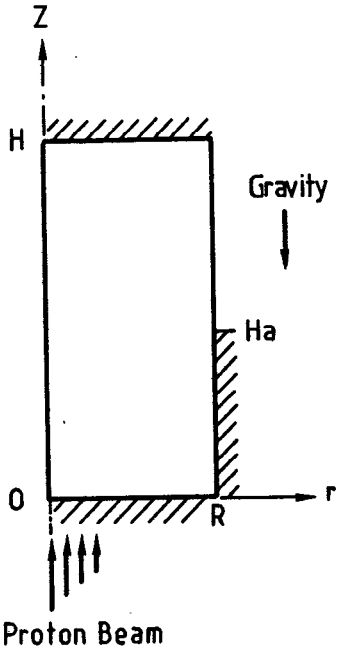

Fig. 1
Schematic of target and coordinate system.

2.2 Basic equations

The basic equations are the coupled partial differential equations of continuity, momentum and energy. However, in this work, these were transformed to equations of vorticity by applying the ROT-operation and introducing the stream function. They are then expressed in dimensionless form by normalization (see appendix) to give:

$$\frac{\partial \Omega}{\partial t} + \gamma V_r \frac{\partial \Omega}{\partial r} + \gamma V_z \frac{\partial \Omega}{\partial z} - \gamma V_r \frac{\Omega}{r}$$

$$= Pr \left[-\gamma \frac{\Omega}{r^2} + \frac{\gamma}{r} \frac{\partial \Omega}{\partial r} + \gamma \frac{\partial^2 \Omega}{\partial r^2} + \frac{1}{\gamma} \frac{\partial^2 \Omega}{\partial z^2} \right] - Pr^2 Gr \frac{\partial T}{\partial r} \qquad (1)$$

$$\frac{\partial T}{\partial t} + \gamma V_r \frac{\partial T}{\partial r} + \gamma V_z \frac{\partial T}{\partial z} = \frac{\gamma}{r} \frac{\partial T}{\partial r} + \gamma \frac{\partial^2 T}{\partial r^2} + \frac{1}{\gamma} \frac{\partial^2 T}{\partial z^2} + \Phi \qquad (2)$$

$$\Omega = \frac{\gamma^2}{r^2} \frac{\partial \Psi}{\partial r} - \frac{\gamma^2}{r} \frac{\partial^2 \Psi}{\partial r^2} - \frac{1}{r} \frac{\partial^2 \Psi}{\partial z^2} \qquad (3)$$

where Pr is the Prandtl number ($= \nu/\alpha$), and Gr the Grashof number ($= g\beta T_0 L^2 d/\nu^2$).

The stream function is related to the fluid velocities by

$$V_z = \frac{1}{r} \frac{\partial \Psi}{\partial r} \quad , \qquad V_r = - \frac{1}{r} \frac{\partial \Psi}{\partial z} \qquad (4)$$

Through this relationship the continuity equation is automatically satisfied.

2.3 Boundary and initial conditions

Boundary conditions for the stream function are taken as

$$\Psi = \frac{\partial \Psi}{\partial z} = 0 \quad ; \; z = 0\&1 \quad 0 < r < 1 \tag{5}$$

$$\Psi = \frac{\partial \Psi}{\partial \Psi} = 0 \quad ; \; r = 0\&1 \quad 0 < z < 1 \tag{6}$$

$$\frac{\partial T}{\partial r} = 0 \quad ; \; r = 0 \quad 0 < z < 1$$
$$r = 1 \quad 0 < z < Ha \tag{7}$$

and the thermal boundary conditions are

$$T = 0 \quad ; \; r = 1 \quad Ha < z < 1 \tag{8}$$

$$\frac{\partial T}{\partial z} = 0 \quad ; \; z = 0\&1 \quad 0 < r < 1 \tag{9}$$

where Ha is the length of the adiabatic surface as defined in Fig. 1.

Since vorticity boundary conditions cannot be given, they are approximated with the values at the next inside grid points and corrected by iteration.

Initial conditions were determined from the assumption of having a quiescent liquid with a uniform temperature (the melting temperature of LBE)

$$V_r = V_z = \Psi = \Omega = T = 0 \text{ at } t = 0 \tag{10}$$

Most of the calculations were carried out with a boundary condition of the full length of the side wall at a constant temperature (conducting wall, Ha = 0).

2.4 Profile of heat generation

As the driving force for the fluid motion of the target liquid is only the buoyancy force due to the internal heat generation, and no external temperature difference is applied to the system, the

profile of heat generation needs to be approximated fairly well. For these calculations the empirical formula for the volumetric energy deposition [4] was used. The formula is expressed as:

$$q(r,z) = \frac{5.7 \times 10^6 \times I}{(\sigma_o + 0.04\ z)^2}\ e^{-\left(\frac{r}{\sigma_o + 0.04\ z}\right)^2}\ e^{-\frac{z}{30}} \qquad (11)$$

where r and z are position variables in cm unit, I beam current in Ampères and σ_o is a parameter which was determined experimentally as 1.6 cm.

2.5 Numerical calculation

For solving the time dependent equations, (1) to (3) above, the finite difference technique was used. The normal centred differencing formula was mainly used, but the so-called upwind difference scheme was used for the inertial terms in equations (1) and (2). The vorticity and temperature equations were solved by the Alternating Directional Implicit (ADI) method and the stream function equation by the Successive Over Relaxation method (SOR). The schematic flow diagram for the calculational procedure is illustrated in Fig. 2. Since all the boundary values cannot be given at some time level simultaneously, the values of results at the preceding time level were used; to correct this approximation, some internal iterations were carried out (II1 to II3 in Fig. 2). Furthermore, to take account of the nonlinearity and coupling of the basic equations, another iteration (II4) was performed. These internal iterations were terminated when maximum changes of values decreased to 0.1 %. The total iteration with respect to time was terminated when the maximum change of stream function decreased to 0.1 % of the value at the preceding time level.

Since the limit of numerical stability of the ADI method has not yet been formulated in a general manner, the time step cannot be determined from a stability condition. From the author's experiences for the present problem, it was found to be quite dependent on the beam power; the higher the beam power, the smaller the time mesh required, otherwise numerical divergence occurred. The time step was kept constant in any one computational run and varied from 1×10^{-5} to 1×10^{-6} (dimensionless).

The number of grid points also cannot be determined from stability analysis. For some cases of target height and beam current, there was no divergence of computation but some apparently false physical solution were obtained. In order to determine the number of grid points several trial computations were performed for the highest beam power and the largest aspect ratio, using grid points of 20 x 20, 40 x 40 and 80 x 80. The results showed sufficiently similar profiles of transient temperature

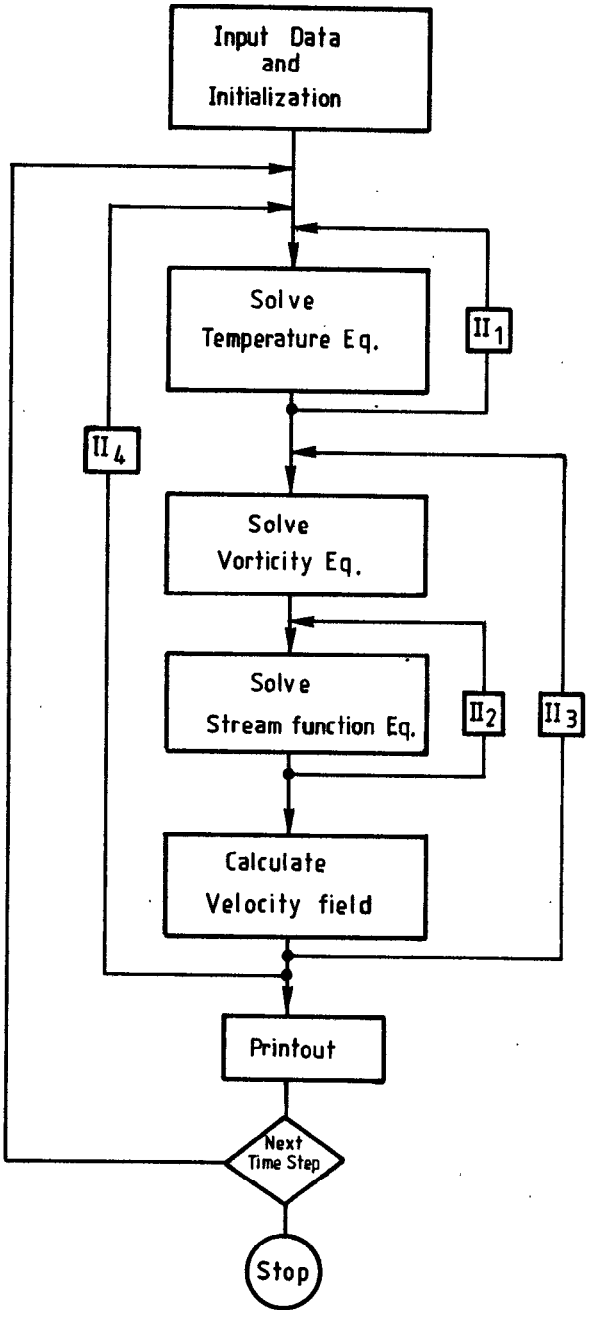

Fig. 2
Flow diagram of numerical calculation

field and stream lines for 40 x 40 and 80 x 80, that 40 x 40 was used in the series of computations.

All the computations were carried out on the SIN VAX-11 computer.

3. RESULTS AND DISCUSSIONS

For most of the computations, the following values are common: a target radius of 15 cm and a beam current of 0.1 mA. The majority of the results are presented as contour maps of stream function and temperature. The contour lines of stream function represent the path of flow of an elemental fluid particle. The outermost contour for both temperature and stream function, correspond to the lowest values (= dT and $d\Psi$), and these values are also used as the interval between the lines. Explicit values of dT and $d\Psi$ are given in the figure captions.

3.1 Transient behaviours

3.1.1 Streamline field and temperature profile

Figure 3 shows the transient temperature distributions and streamline fields for a 150 cm high target with side wall cooling.

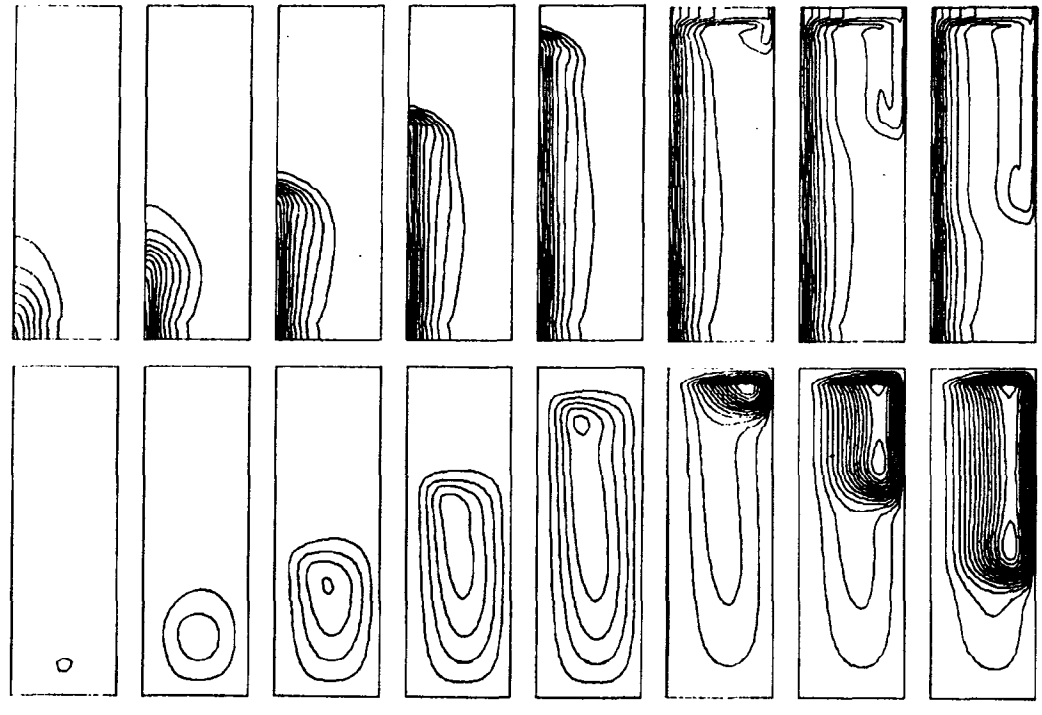

Fig. 3
Transient behaviour for a 150 cm high target. Beam current is 0.1 mA. Contour lines are for dT = 0.05 (6.3 ^{o}C) for temperature in (a) to (m), 0.025 (3.1 ^{o}C) in (n) to (p), and with $d\Psi$ = 10 for streamline. (a) is at 1.2×10^{-4} (3.8 sec) and the time interval is 8×10^{-5} (2.5 sec).

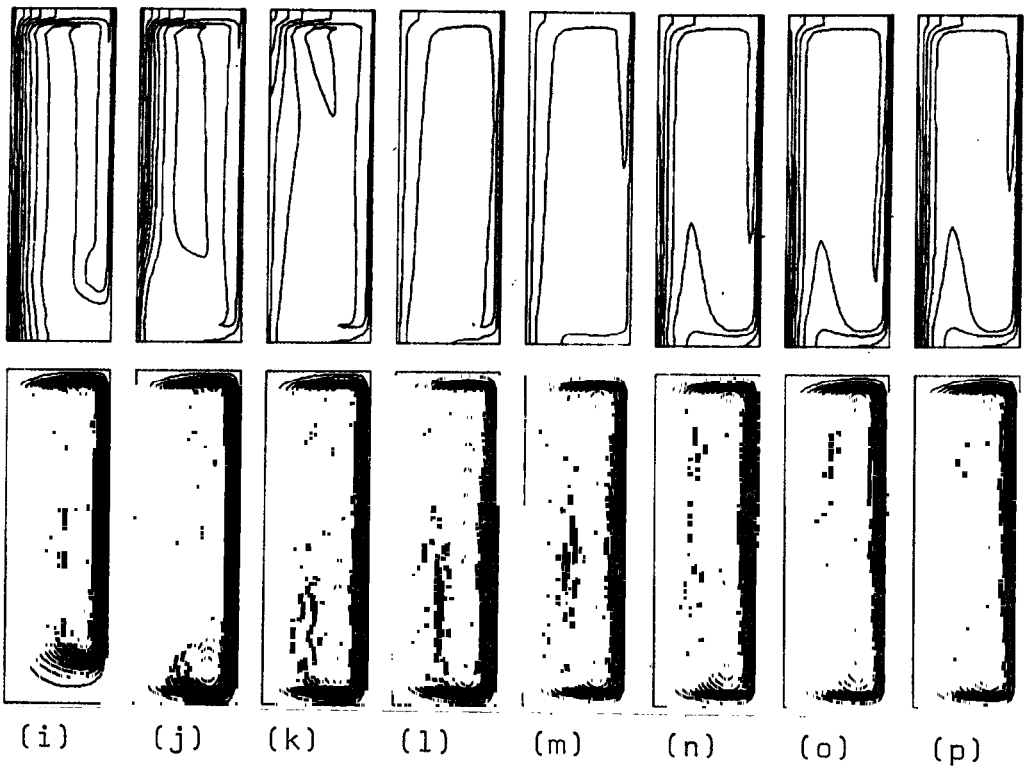

Fig. 3 (continued)
(i) is at 7.6×10^{-4} (24.2 sec) and interval is also 8×10^{-5} (2.5 sec).

It shows clearly the process of generation and growth of circulation (a - h). At (a - b), a clockwise circulation starts in the lower portion of the container where most of the energy is deposited. As time proceeds, the circulation grows (the number of contour lines increases) and the centre of the roll rises. When this roll reaches the top, it grows rapidly. A second roll appears (g), grows and moves downwards elongating the total circulation (g - j). The coexistence of these two rolls lasts until the second reaches the bottom, when they both merge into the total circulation (j - m), giving a stable laminar flow by time step (n).

The distribution of temperature follows the above mentioned changes of streamline fields. At first the flow is so small that the temperature distribution is similar to the profile of internal heat generation. But at (b), the bottom part of the distribution shrinks, since cold liquid flows inward due to the circulation. As time proceeds, this shrinkage spreads upwards, following the rise of the roll, resulting in a vertical hot column around the centre line (vertical and parallel contour lines). The presence of a very weak secondary roll leads to the slight distortion of the temperature distribution (c - e).

A stronger effect can be seen from the first roll in figures (f) - (h). At the top of the container the strong local circulation makes the isothermal lines horizontal transporting heat from the central region to the periphery. Following the downward motion of the second roll, the hot liquid column (which is partially cooled at the surface) flows down, leaving the intermediate region (core) between the central hot column and surface at low temperature (g - i). When the second roll reaches the bottom (j), this core becomes an island of lower temperature. During the time when the two rolls are merging and the total circulation is growing, the central hot column is washed away and the position of the temperature maximum moves from the bottom centre to the top centre (j - l), and a relatively uniform temperature distribution is formed (l - m). However, once the total circulation is established, the heat is accumulated around the centre line and forms the central hot column again (n - p). The maximum temperature is also at the bottom centre. The high temperature gradient due to the side-wall cooling can also be seen.

This general aspect of temperature profile and streamline field agrees well with the experimental and numerical investigation by Torrance et al. [5]. Their work was done for natural convection of air in a cylindrical container of unit aspect ratio (but with local heating at the bottom surface) and, in particular, showed the "vortex shedding" during the transient phase for a high Grashof number system.

3.1.2 Time change of temperature

Figure 4 shows the change of temperature with time for a 150 cm high target. T_{max} is the maximum temperature in the system while the others are at fixed points. The total length of time is 1.68×10^{-3}. The maximum temperature increases very quickly to about 75 ^{o}C above the melting temperature. It then drops, reaching a stable value of 26 ^{o}C after some weak oscillations. The position of the maximum temperature is mainly located at the bottom centre of the target, but during the drop, it moves up the centre line.

Temperatures at the fixed points show a similar behaviour to that of the maximum; an increase followed by a decrease with a somewhat flat "plateau" inbetween. The starting time of the temperature increase is earlier and its "plateau" value is larger, the closer the point is to the bottom centre. This behaviour of the temperature can be understood as follows: At first, the hot fluid heated by the beam flows up and increases the temperature at these points, and then, as the flow is being established cold fluid is carried in from the peripheral regions to decrease the temperature. For the lower portion of the target, the small overshoot at the start of the "plateau" might be caused by the devel-

opment of the flow; this indicates that it may be possible to monitor the degree of development of the main flow by observing the temperature change at points in the lower part of the target.

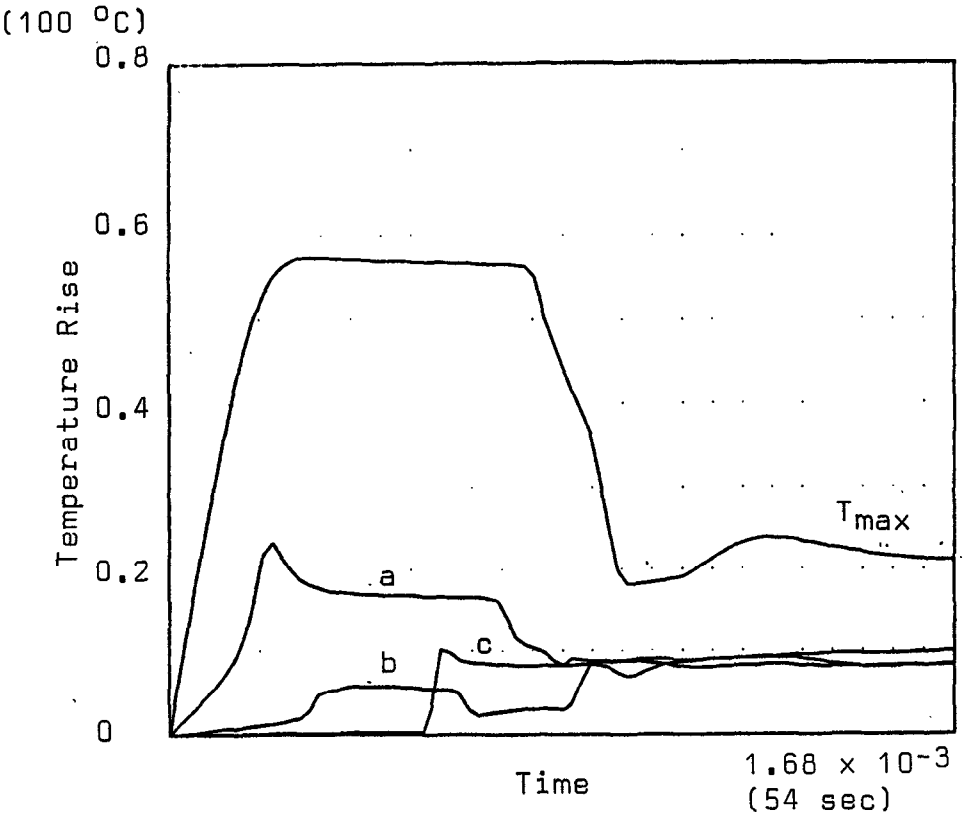

Fig. 4
Change of temperature with time.
T_{max}: maximum temperature in the whole system.
(a): Temperature is at the fixed point r = z = 0.25; (b) at r = z = 0.5; (c) at r = z = 0.75. The time range is from 0 to 1.68×10^{-3} (54 sec)

3.1.3 Energy flow

Figure 5 is a vectorial representation of energy flux shortly after the start of heating:
Fig. 5 (a) shows the contribution from heat conduction,
(b) convection and,
(c) the total energy flux.

The main contribution to the energy flow from the heated region comes from convection, even at this early stage, as is illustrated by the similarity of Fig. 5 (b) and Fig. 5 (c). Convection completely dominates conduction at later stages. Figure 6 shows the change of

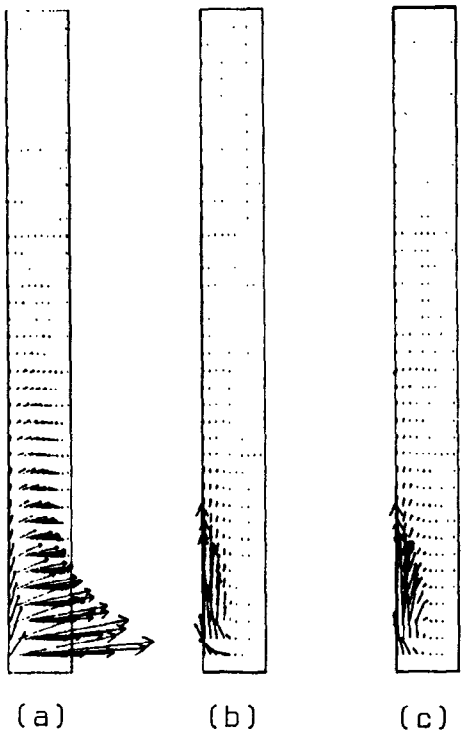

Fig. 5

Vectorial energy flux for 150 cm high target, current = 0.1 mA and at time = 2×10^{-5} (0.64 sec)
(a) conduction
(b) convection
(c) total
These figures are normalized in each frame independently, and there is no relationship in length of arrows between the three.

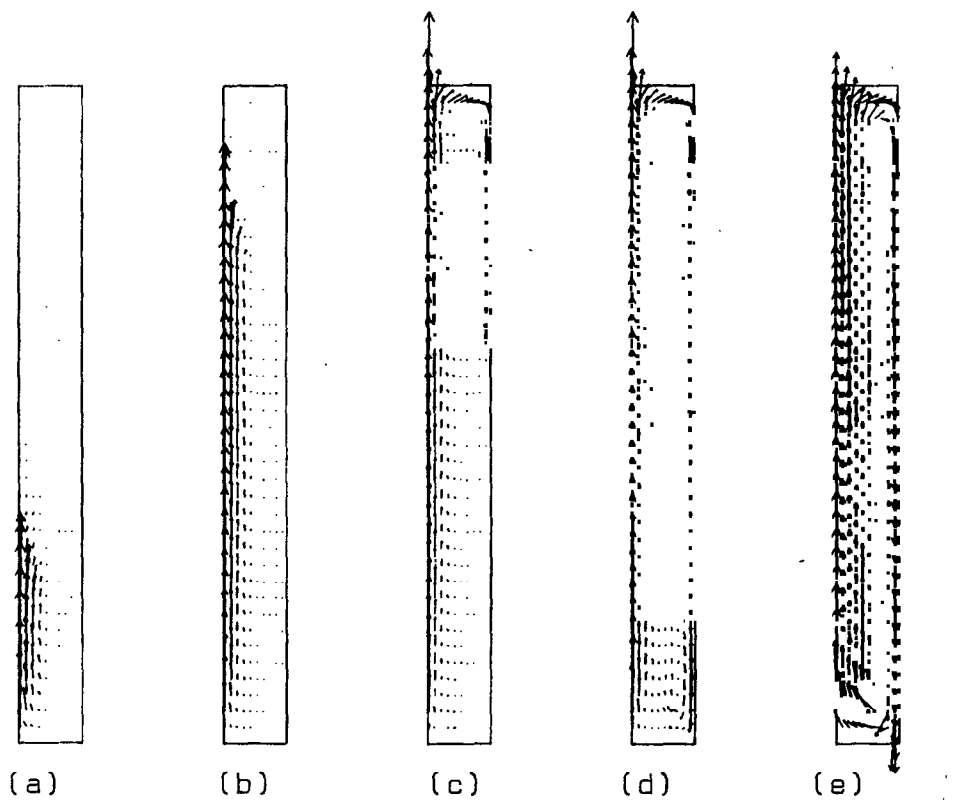

Fig. 6
Change of vectorial energy flux. Calculational parameters are the same as in Fig. 5. (a) is at 2×10^{-4} (6.4 sec), and the time interval between successive diagrams is 2×10^{-4} (6.4 sec).

the total energy flux with time. The change of the energy flow is fairly large, and follows the development of the liquid flow. When the flow is established, the energy flows towards the centre line in the bottom regions of the target and towards the periphery at the top. In the middle region of the target, the energy flows vertically upward in a central column transporting the deposited energy to the top. This heat is then transferred to the cooled wall during the downwards flow in the outer region of the target.

3.2 The effects of physical conditions

3.2.1 Target height

Figure 7 gives a comparison of the profiles of temperature distribution and streamline fields for various target heights at one fixed dimensionless time (1.6×10^{-3}). By this time, the total circulation is well established for all three cases. The value of stream function is largest for the shortest target. The general features of the temperature distribution are the vertical isotherms in the central and peripheral regions, horizontal isotherms in the top region, and a fairly uniform temperature distribution in the intermediate core. Inversion layers are generated by the total circulation at the top centre and the bottom periphery, indicating some possibility of the appearance of the stagnation at the bottom corner. From this general behaviour, (but bearing in mind the fundamental limitations in the calculation), we could expect that in the main part of the container a stable laminar flow develops, which is part of a total circulation throughout the target and is effective for energy transport.

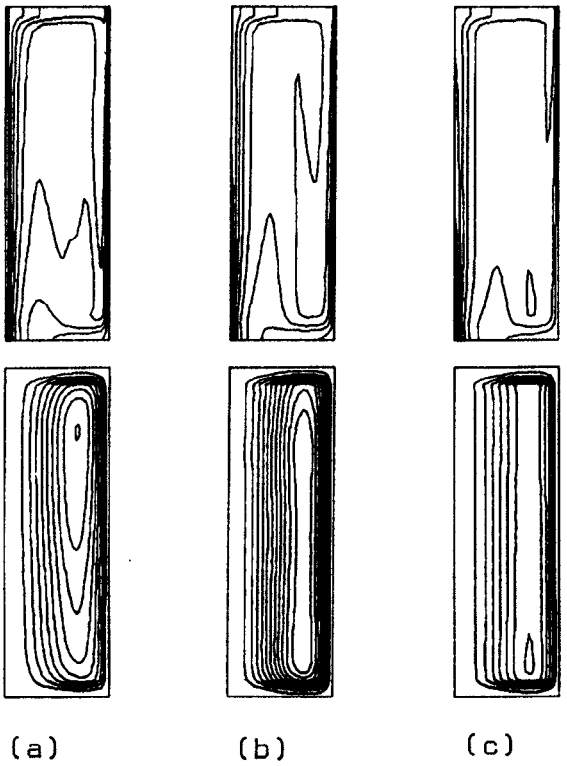

Fig. 7
Change of temperature (top) and flow (bottom) profiles with target height;
radius = 15 cm
current = 0.1 mA
(a) 75 cm at 26.1 sec
(b) 150 cm at 52.2 sec
(c) 300 cm at 104.5 sec
(1.64×10^{-3} for all)
Contour lines are with
$dT = 0.025$ (3.1 °C) and
$d\Psi = 10$

3.2.2 Beam power

Calculations were performed with various beam currents for a target height of 150 cm. Beam currents of 0.1, 0.5 and 1 mA were used. Profiles for temperature and streamlines are very similar although the absolute values of these are different. The significant difference is that the speed of rising of the roll is somewhat larger for higher beam currents. This is caused by the larger buoyancy forces due to the higher temperature difference. The highest temperatures in the container were found at the bottom centre for all three cases, and the values are plotted as a function of beam current in Fig. 8. A power law relationship between maximum temperature rise and beam current was found, and an estimate of the exponent is 0.68, which is in very good agreement with the value of 2/3 given by a simple one-dimensional analysis [6]. This relationship is helpful in estimating the maximum temperature for other beam currents.

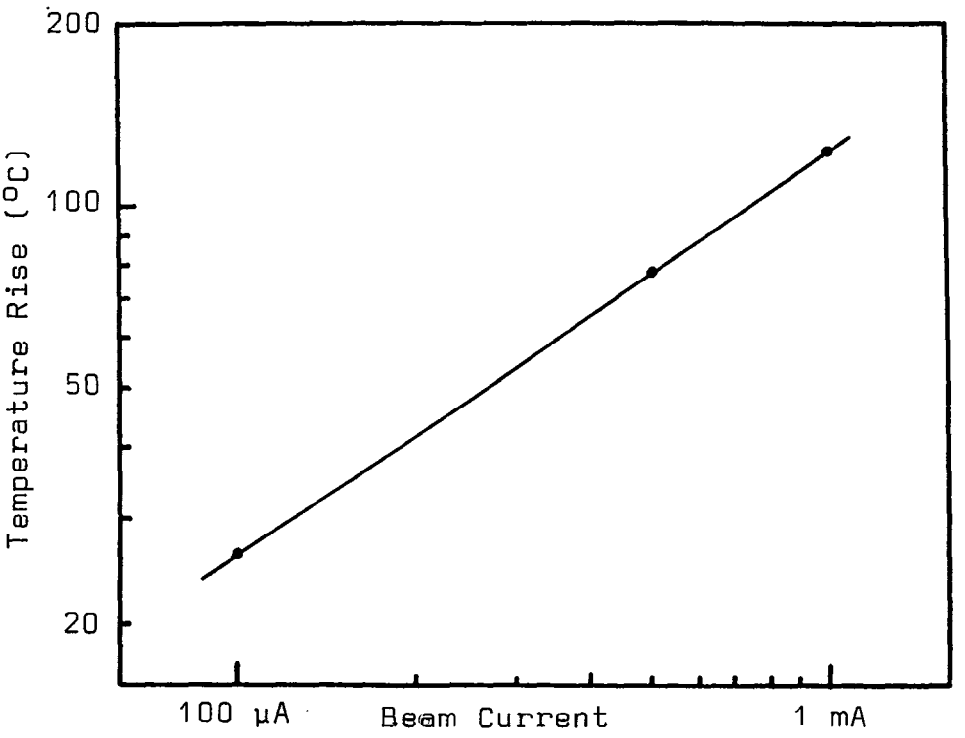

Fig. 8
Maximum temperature rise versus beam current

3.2.3 Adiabatic side wall

Calculations were done with the lower half of the side wall adiabatic, for two target heights (150 and 300 cm), in order to see if a simpler arrangement for the target is feasible. All other

conditions and parameter values are the same as for the case with a conducting side wall. The temperature distribution and streamline field are shown in Fig. 9. The general structure of the flow

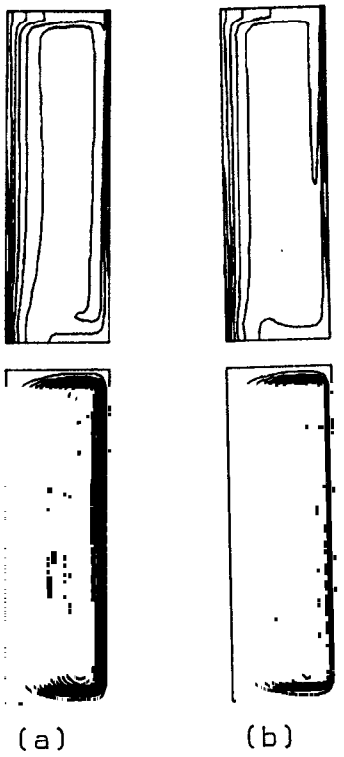

Fig. 9
Temperature (top) and flow (bottom) profile for adiabatic side wall condition;
(a) Ha = 75 cm
(b) = 150 cm
Physical parameters are all the same as in Fig. 7.
Contour lines are with
dT = 0.025 (3.1 ^{o}C) and
dΨ = 10

patterns are very similar to the cooled side wall cases (see Fig. 7), with the absolute values of stream function larger in the upper region implying a stronger circulation. The temperature distributions show more significant differences. The temperature gradients are smaller beside the adiabatic surface, which is obviously from the difference of boundary condition, and also leads to the simpler temperature profile in the lower peripheral and core regions. Because the area of heat transfer out of the target is reduced, the temperature in the central column is higher. At the end of the calculations the maximum temperature rises above the melting point were 35.9^{o}C for 150 cm target and 32.8^{o}C for 300 cm, whereas they are 26.0^{o}C and 25.2^{o}C respectively, for conducting walls.

4. CONCLUSIONS

Numerical investigations have been made for the natural convection in a liquid lead-bismuth target based on the conventional Boussinesq approximation. Geometrical configurations were restricted to vertical cylinders of various lengths. A distributed internal heat generation was taken into account and is the only driving force for liquid motion. The following conclusions are made:

1) In the transient phase, the flow bifurcated but did not lead to a hydrodynamic instability.
2) Following the initial transient phase, a stable total circulation is established in all the cases examined.
3) The temperature profile shows that there is a hot column of liquid about the centre line and a steep gradient at the surface. In the intermediate core region, the temperature variation is small.
4) The position of the maximum temperature in a target is at the bottom centre, i.e. at the middle of the beam entry window, except for a short period in the transient.
5) This maximum temperature rise in the transient is several times higher, depending on the systems, than that of the stationary value.
6) The maximum temperature rise in the system is directly proportional to (beam power)$^{0.68}$.
7) Calculations with an adiabatic side wall of half the length of the target show the accumulation of small amounts of heat in the insulated region of the system, resulting in a higher maximum temperature at the bottom center.

ACKNOWLEDGEMENT

The author is grateful to Dr. W.E. Fischer, F. Atchison and Dr. Ch. Tschalär for their helpful discussions and encouragements.

REFERENCES

[1] W.E. Fischer, Status Report on the SIN Neutron Source, These proceedings
[2] H. Hoffmann, Proceedings ICANS-V, Jülich
[3] Y. Takeda, to be published
[4] L. Buth and H. Werle, INR-996, Kernforschungszentrum Karlsruhe (1980)
[5] K.E. Torrance and J.A. Rocket, J.Fluid Mech., Vol. 36 (1969) p. 21 and 33
[6] Ch. Tschalär, Proceedings ICANS-V, Jülich

NOMENCLATURE

H	: Target height	z	: Axial coordinate
Ha	: Height of adiabatic wall	γ	: Aspect ratio (= H/R)
R	: Target radius	Ω	: Vorticity
r	: Radial coordinate	Ψ	: Stream function
t	: Time	ϕ	: Internal heat generation
T	: Temperature	Gr	: Grashof number
V_r	: Radial velocity	Pr	: Prandtl number
V_z	: Axial velocity	β	: Thermal volume expansion coefficient

APPENDIX

The physical variables (shown with *) were normalized in the following way:

t	$= \alpha t^*/HR$	V_z	$= R^2 V_z^*/H\alpha$
Ψ	$= \Psi^*/H\alpha$	z	$= z^*/H$
V_r	$= RV_r^*/\alpha$	T	$= (T^*-T_o)/T_o$
r	$= r^*/R$	Φ	$= HRq/(\alpha T_o\ \rho C_p)$
Ω	$= HR\ \Omega^*/\alpha$		

where α is the thermal diffusivity and T_o the melting temperature, ρ the density, C_p the specific heat of LBE and q the power density.